We are IntechOpen, the world's leading publisher of Open Access books Built by scientists, for scientists

4,800
Open access books available

122,000
International authors and editors

135M
Downloads

Our authors are among the

154
Countries delivered to

TOP 1%
most cited scientists

12.2%
Contributors from top 500 universities

CLARIVATE ANALYTICS BOOK CITATION INDEX INDEXED

WEB OF SCIENCE™

Selection of our books indexed in the Book Citation Index in Web of Science™ Core Collection (BKCI)

Interested in publishing with us?
Contact book.department@intechopen.com

Numbers displayed above are based on latest data collected.
For more information visit www.intechopen.com

6

Determination of Near-Neighbour Bonding in the Mn-Implanted GaSb Crystals

Anna Wolska
Institute of Physics, Polish Academy of Sciences
Poland

1. Introduction

Ion implantation is a powerful technique for the production of new materials. However, in order to find an optimal way of obtaining compounds with desirable properties, the influence of many parameters must be tested. The characterization, among other things, should contain a very precise determination of the local neighbourhood of the implanted ions. This can be revealed by the X-ray absorption fine structure (XAFS) techniques. Their main advantage is elemental selectivity, which allows the experimenter to extract information on the atomic neighbourhood of the chosen species of atom even at very low concentration of this element.

2. X-ray absorption fine structure techniques

When the X-ray photon energy is equal to the binding energy of a core level of an atom in the material an abrupt increase in the absorption coefficient occurs. This phenomenon is known as the absorption edge. The edge energy is characteristic for the type of the excited inner shell and the type of the absorbing element.

The X-ray absorption spectrum is being usually divided into two regions: X-ray absorption near edge structure (XANES) up to around 50 eV above the edge and extended X-ray absorption fine structure (EXAFS) which starts around 50 eV and can reach even 1000 eV above the edge. However, the exact energy dividing both regions depends mainly on the investigated system.

Detailed description and interpretation of the XAFS processes can be found in many books and papers (Eisenberger & Kincaid, 1978; Koningsberger & Prins, 1988; Lee et al. 1981; Stohr, 1996; Teo, 1986; Teo. & Joy, 1981). Here only very simple explanation is provided. The photoelectron created during the X-ray absorption process can be represented as an outgoing wave which is scattered by the surrounding atoms. The outgoing and scattered waves interfere with each other which modifies the absorption coefficient in a way that depends on the type and spatial arrangements of the neighbouring atoms. Such pattern does not appear for an isolated atom.

In XANES multiple scatterings dominate. The shape of a spectrum in this region depends not only on the radial distances, the angles between the atoms, their type and number but

also on their chemical bonding. Different chemical bondings (ionic, covalent, metallic) alter core-level binding energies producing absorption edge shifts and changing the distribution of the unoccupied states above the Fermi level. As an example the measurements of the manganese oxides at the Mn K edge can be considered. Fig. 1 presents the XANES spectra for Mn, MnO, Mn_2O_3 and MnO_2. It can be noticed that the edge position moves toward higher energy while the Mn atoms ionicity changes from 0 to IV. Studies presented by Croft et al. 1997 showed that in case of the Mn K edge the edge position changes linearly with the valence state. However, not only the edge position but also the shape of the spectra changes together with the rearrangements of the atoms around the absorber, reflecting the change in the local density of states.

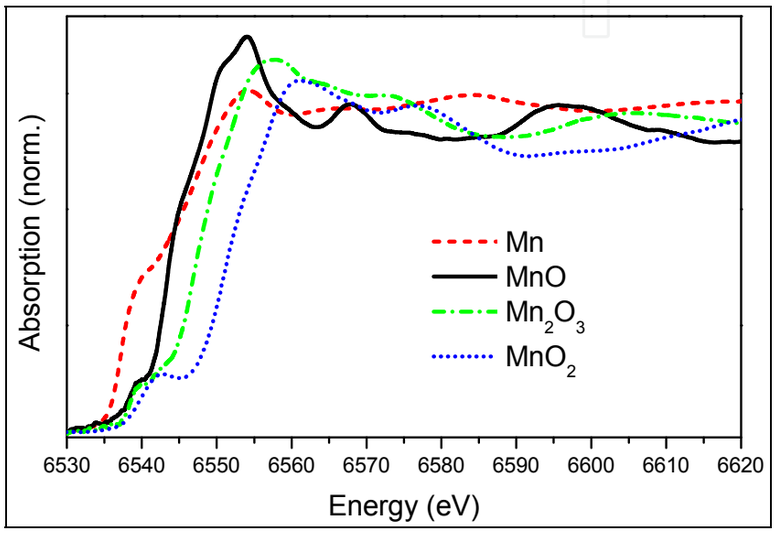

Fig. 1. XANES spectra at the Mn K-edge of the Mn foil and manganese oxides.

In the EXAFS region single scatterings dominate which simplifies the analysis. Fig. 2a shows the EXAFS spectrum of MnO. As can be noticed, at the end of the range, the oscillations are very weak. The absorption coefficient can be defined as $\mu(E) = \mu_0(E) * (1 + \chi(k))$, where $\mu_0(E)$ represents a smooth atomic background and $\chi(k)$ represents the EXAFS oscillations. By using this equation $\mu(E)$ can be converted into $\chi(k)$. The result is shown in Fig. 2b. These oscillations include information about the type, number and distances of the neighbouring atoms. The next step is to perform Fourier transformation (FT) from k (photo-electron wavenumber) to R (real) space. The $\chi(R)$ is a complex function; in the Fig. 2c the magnitude and the real part for MnO spectrum are shown. The positions of the peaks are related to the distances between the absorber and its neighbours. The amplitude and shape of the peaks depend on type and number of neighbouring atoms. E.g. the first peak in the plot consists of 6 oxygen atoms at a distance R = 2.2 Å, while in the second one 12 Mn (R = 3.14 Å) and 8 O (R = 3.85 Å) atoms are located. In order to analyse this kind of data a realistic model should be assumed first, and then the fitting of this model to the experimental data should be performed. The fitting parameters include the distance between given coordination shell and the absorbing atom; the number of the atoms in a given shell as well as static and thermal disorder. The thermal disorder can be reduced by performing the measurements at liquid nitrogen temperature.

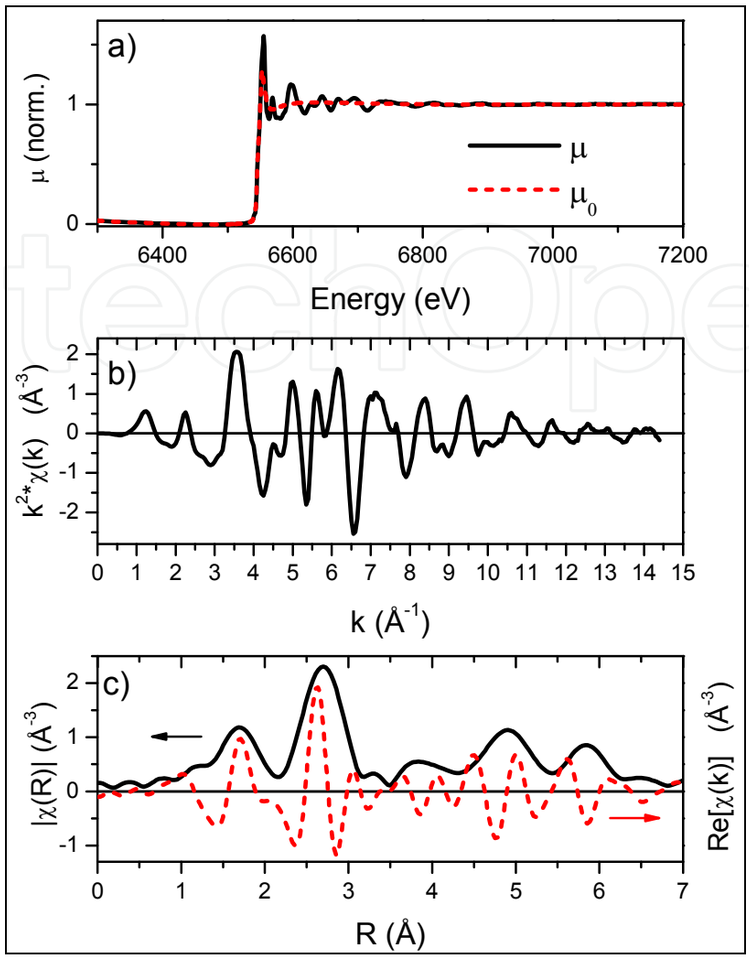

Fig. 2. a) EXAFS spectrum of MnO at the Mn K-edge; b) EXAFS oscillations extracted from a) after atomic background removal; c) the magnitude (black solid line) and the real part (dashed red line) of the FT EXAFS oscillations from b).

The fitting can be done using several accessible programs e.g. SixPACK, EXCURVE, WinXAS. The analysis presented in this chapter was conducted using IFEFFIT data analysis package with Athena and Artemis programs (Ravel & Newville, 2005).

The XAFS techniques are selective (only the selected element is investigated), local (only the closest surrounding of the absorbing atoms is investigated, up to 10 Å for perfectly ordered structures) and sensitive (even very low concentration of the element can be detected). Moreover, they can be used for samples in different states: solids (crystalline or amorphous), liquids, solutions or gaseous. However, it should be emphasized that if the investigated atoms form different compounds, the data obtained from the XAFS experiment is averaged over all those neighbourhoods.

3. Materials

The interest in granular materials composed of semiconductor matrix with nanoinclusions of magnetic materials is rapidly growing due to the demonstration of their usefulness in the

construction of magnetic tunnel junctions with huge magnetoresistance. (Hai et al., 2009) In this kind of material, small ferromagnetic nanoparticles are immersed in the semiconductor host lattice providing a built-in local magnetic field. However, in case of MnAs precipitates, two crystalline structures with different magnetic properties were found: the cubic zinc blende type and hexagonal one. This obstacle does not exist for MnSb clusters since they have only hexagonal form. Another advantage of MnSb is a T_C well above room temperature. It was shown that bulk MnSb has a T_C of 587 K (Panchula et al., 2003) while for MnAs it is only 318 K. What's more, the magnetic force microscopy (MFM) as well as superconducting quantum interference device (SQUID) measurements revealed the existence of magnetic anisotropy for the MnSb inclusions grown by the MBE method. The X-ray magnetic circular dichroism (XMCD) experiment also confirmed that the direction of the easy magnetization axis in GaSb:MnSb granular layers grown on the GaSb(100) substrates was close to the in plane direction. The ratio of orbital to spin momentum depends on the shape and size of inclusions. (Lawniczak-Jablonska et al., 2011) In the case of small inclusions the enhancement of orbital momentum was observed which offers interesting opportunities for magnetic applications in a low dimensional limit. The observed change in the direction of the easy magnetization axis indicates on the possibility to control it by proper choice of the substrate and growth conditions. These results show that a compound consisting of MnSb inclusions and semiconductor matrix exhibits very interesting magnetic and structural properties which can be used in the construction of the spintronic devices. Finding the way of forming this kind of material by the implantation method could increase its variety of applications.

3.1 Implantation with low energy Mn^+ ions (10 keV)

The GaSb (100) crystals implanted with low energy Mn^+ ions were considered first. The implantation energy was equal to 10 keV and the doses of the Mn^+ ions were: $1x10^{16}$ Mn/cm^2 (#1 sample), $2x10^{16}$ Mn/cm^2 (#2 sample) and $3x10^{16}$ Mn/cm^2 (#3 sample). After the implantation all samples were annealed in a vacuum furnace at 650 ^oC for 10 min.

The depth profiles of the element distribution in sample #2 as measured by the secondary ion mass spectroscopy (SIMS) are shown in the Fig. 3. Only the region very close to the surface is disturbed by the implantation which, for this technique, is almost below the edge of detection. However, still it is an indication that the Mn atoms concentrate close to the surface as it was expected in this case.

The shapes of the XANES spectra after normalization look almost the same, which indicates that the Mn atoms are located in the similar positions independently on the applied dose. Since the aim of the implantation was to form the MnSb inclusions, the spectrum of powdered MnSb was measured as well. It can be seen in Fig. 4 that the spectrum of the standard MnSb sample is completely different from the spectra of the implanted samples. This excludes the possibility of MnSb formation in the investigated samples. On the other hand, the strong first peak is characteristic for MnO. The other maxima for the #1 sample in comparison to MnO are weaker and slightly shifted in energy which means that other type of compound dominates here. However, existence of some amount of manganese oxides cannot be excluded.

From EXAFS analysis more detailed information about the distribution of the atoms can be found. XANES spectra revealed that there is no MnSb, therefore, other cases should be

considered. As it was predicted, the MnO structure does not dominate here. Oxygen can be only responsible for the tail visible between 1 and 2 Å (see Fig. 5). Therefore, other models should be checked.

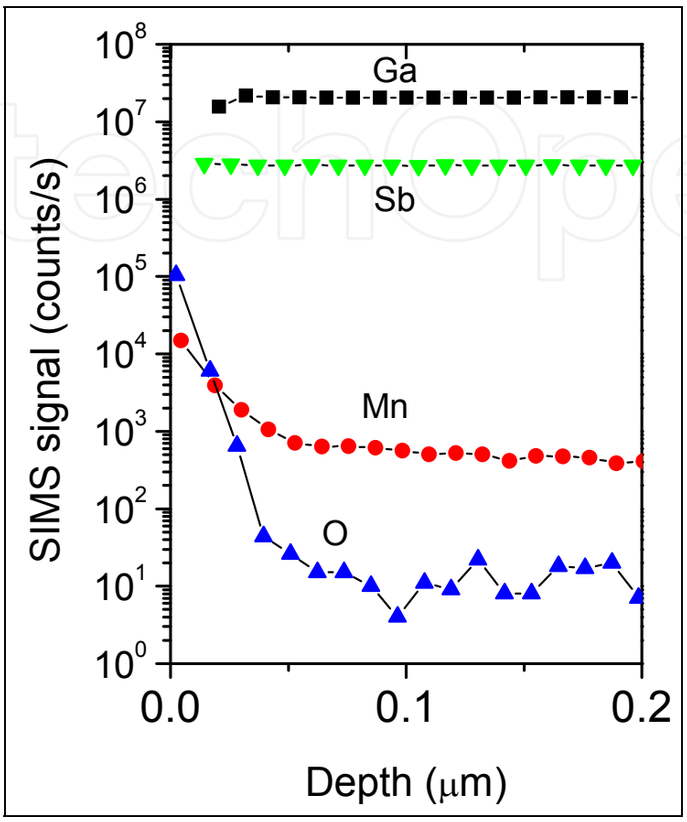

Fig. 3. SIMS depth profiles of the element distribution in the #2 sample.

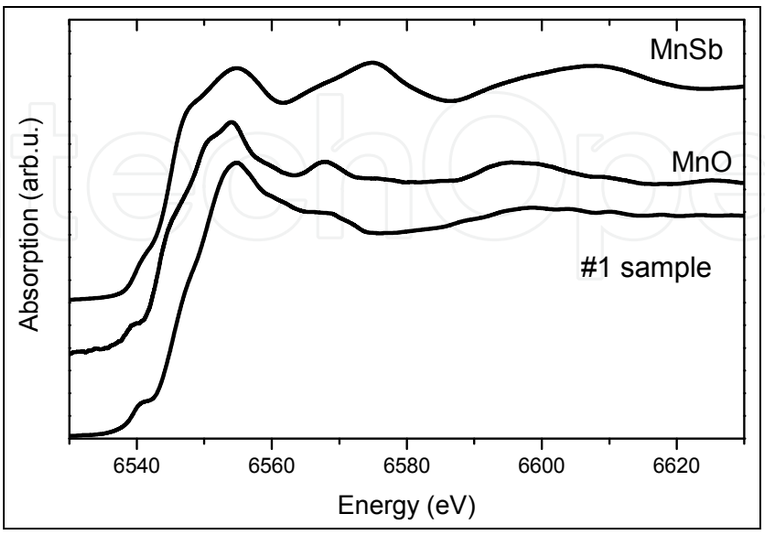

Fig. 4. XANES spectra of the #1 sample compared with the MnSb and MnO references. Spectra are shifted vertically for clarity.

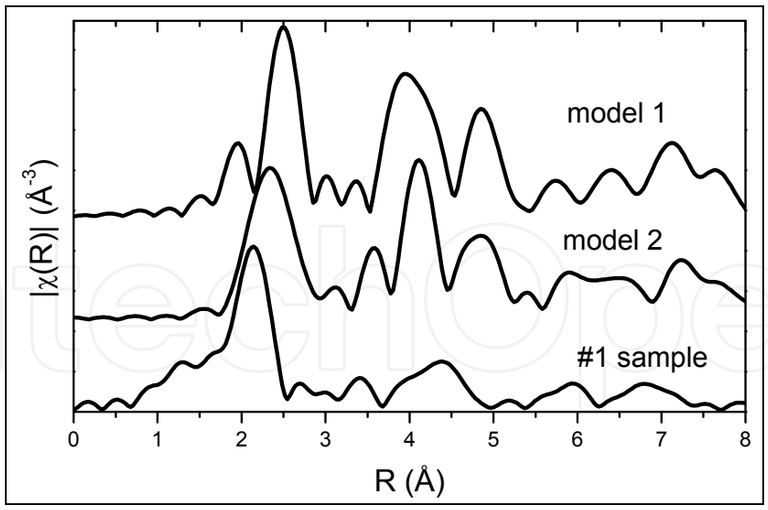

Fig. 5. FT EXAFS spectrum of the #1 sample and theoretical models based on the GaSb crystallographic data. Model 1: Mn substituting Ga (Mn_{Ga}); Model 2: Mn substituting Sb (Mn_{Sb}). Spectra are shifted vertically for clarity.

Since the Mn atoms are implanted into the GaSb crystal, the GaSb model seems to be the obvious choice. First, two cases have to be checked: 1) the Mn atom substituting the Ga atom in the GaSb structure (Mn_{Ga}) and 2) the Mn atom substituting the Sb atom (Mn_{Sb}). Fitting of both models returned unphysical parameters. Therefore, in Fig. 5, not the fitting results but the simulated spectra for the models are compared with the magnitude of FT EXAFS oscillations for the sample with the lowest dose (#1). Model 1 is a sum of 8 single scattering paths corresponding to the consecutive 4 Sb and 4 Ga coordination spheres in the GaSb crystal, where central Mn atom is located in the Ga position. The number of atoms in each coordination sphere was kept set according to the GaSb crystallographic data. Model 2 presents such sum for the Mn central atom located in the Sb position.

A closer look at the calculated spectra for models reveals the possibility that the Ga atoms can be located in the first shell but at shorter distance. Moreover, it seems that the Sb atoms are not located in the vicinity of the Mn atoms. It leads to model 3 also based on the GaSb structure, where only the Ga atoms are present. In Fig. 6 a sum of 4 single scattering Ga paths corresponding to four consecutive shells consisting of Ga atoms is shown. The result seems to be closer to the experimental spectrum but the distances to the subsequent shells are too large. However, with a lack of antimony atoms, it can be expected that remaining Ga atoms rearrange their positions and move closer to the central atom. This is shown in model 4 (Fig. 6), where the distances to each shell were modified to agree with the experiment.

The preliminary fitting of the experimental spectrum was performed using model 3. While defining the parameters, it has to be taken into account that the farther given shell is located in model 3 the more it has to be moved to agree with the experiment. Therefore, the ΔR parameter responsible for monitoring changes in the distances (R) was defined as $R*\alpha$, where α is a parameter measuring lattice contraction. The result is shown in Fig. 7. The fit is not perfect because only single scattering Ga paths were considered, however in spite of that; the model works reasonably well even up to 8 Å. It can be noticed that the distances are getting significantly shorter. The comparison between the distances to the subsequent shells found from model 3 and fit is shown in Tab. 1.

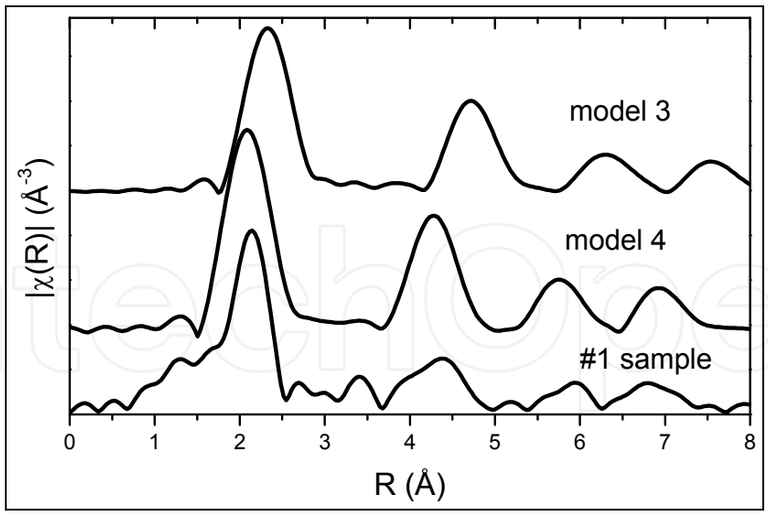

Fig. 6. FT EXAFS spectrum of the #1 sample and theoretical models based on the GaSb crystal with the Sb atoms removed. Model 3: distances to the Ga shells as in the GaSb crystal; Model 4: shortened distances to the Ga shells. Spectra are shifted vertically for clarity.

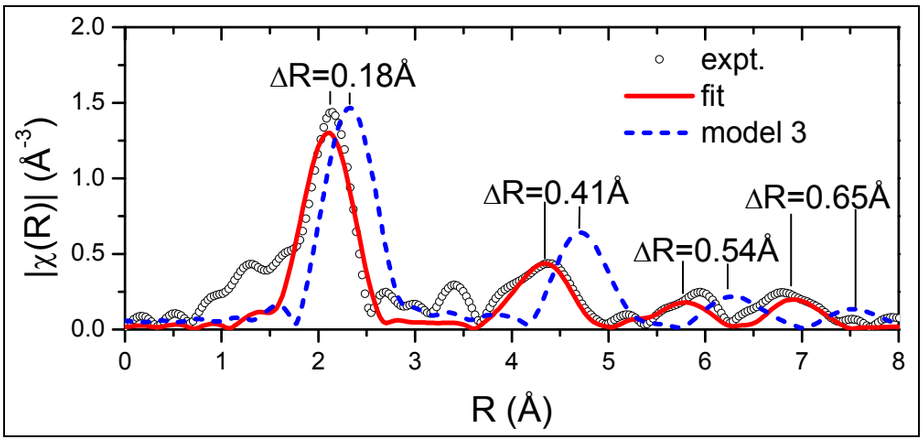

Fig. 7. Fitting of the FT EXAFS spectrum of the #1 sample using single scattering Ga paths for four consecutive Ga spheres in the GaSb crystal compared with the same paths as found from the model 3.

The structure above 5 Å in the spectra for higher doses was not well preserved which indicates that an increase of dose introduces higher disorder in the sample. Therefore, only two Ga shells were considered in the precise fitting. The first and second shells consist of gallium atoms. The tail below the first shell was fitted assuming presence of oxygen. MnO did not crystallize here; only in average 2-3 oxygen atoms at the distance of 2.02 Å were found. In order to further improve quality of the fits also some residual antimony atoms had to be introduced between the shells. In Fig. 8 the results of fitting for samples with all doses are shown.

In summary, the EXAFS analysis revealed that even low energy implantation and quick annealing lead to the significant deficit of Sb atoms around implanted Mn atoms. Some traces of the Mn-O bonds are detected, however, the majority of the Mn atoms is found to be

located in the antimony positions in the GaSb matrix where the Sb sublattice is almost completely destroyed and the remaining Ga sublattice contracts significantly. It leads to the creation of the inclusions containing Mn-Ga material. In these inclusions Mn atoms are located within the contracted Ga sublattice preserving a crystalline order characteristic for the GaSb crystal with the F-43m space group (Wolska et al., 2010).

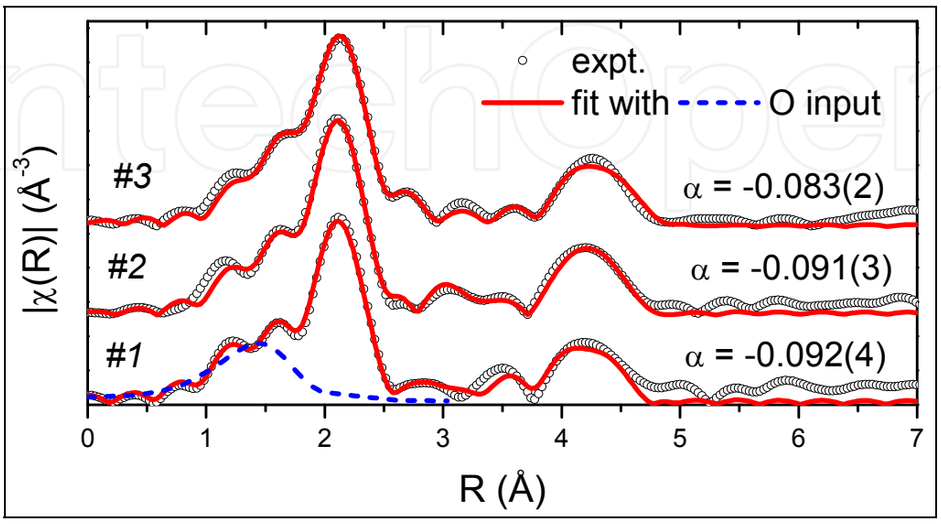

Fig. 8. Fitting results of the FT EXAFS spectra for the implanted samples up to the second coordination shell. Residual O and Sb atoms were also used in the fits. For the #1 sample the contribution from the oxygen atoms is shown (blue dashed line). The α parameter is a measure of lattice contraction. Spectra are shifted vertically for clarity.

	I shell (4 Ga)	II shell (12 Ga)	III shell (12 Ga)	IV shell (16 Ga)
R_{Ga} [Å] (model)	2.65	5.07	6.66	7.95
R_{Ga} [Å] (fit)	2.43	4.66	6.12	7.30

Table 1. The distances to the subsequent Ga shells found from the GaSb model and the fit.

3.2 Implantation with high energy Mn^+ ions (150 keV) at room temperature

The implantation of the low energy Mn^+ ions did not succeed in the creation of the MnSb inclusions. Therefore, in the next step higher energy of the Mn^+ ions was used. The implantation energy was equal to 150 keV and the dose was 1.7×10^{17} Mn/cm^2. One of the samples was left without any additional treatment. The other one was annealed in Ar atmosphere at 350 ^{o}C for 5 min.

The examination of XANES spectra of the samples revealed that this approach was not successful as well. MnSb inclusions were not formed. The XANES spectrum of the as implanted sample is quite shapeless which suggests that the Mn atoms' surrounding is amorphous (see Fig. 9). For the annealed sample weak maxima around 6570 eV and 6600 eV can be distinguished. They correspond to the maxima seen for the samples implanted with low energy ions (in Fig. 9 the #3 sample is shown as an example) described in the previous

procedure. Both spectra are similar, except for the first maximum which is more pronounced for the #3 sample. Since it was attributed to the presence of oxygen, it would imply lack of manganese oxides in the new samples.

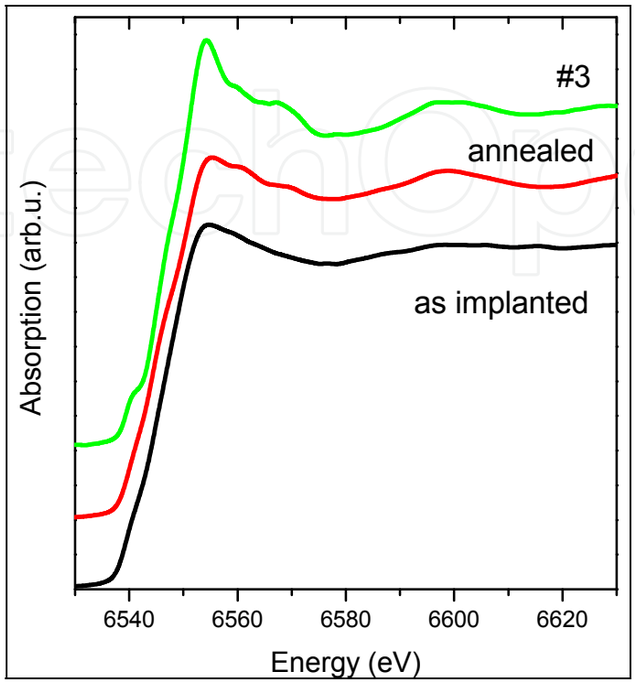

Fig. 9. XANES spectra of the as implanted and annealed samples compared with the #3 sample implanted with low energy ions described in previous subchapter. Spectra are shifted vertically for clarity.

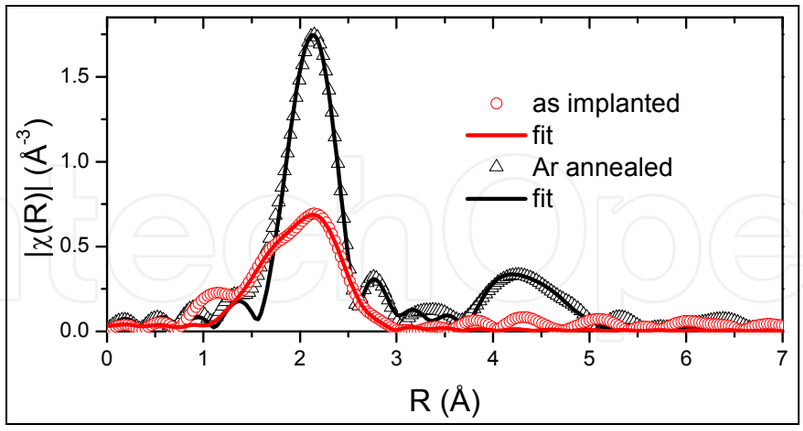

Fig. 10. Fitting results of the FT EXAFS spectra for the as implanted and annealed samples.

In order to obtain more precise information about the Mn location in the samples, the EXAFS analysis was performed. In the FT EXAFS of the as implanted sample only the first shell can be distinguished (Fig. 10). This confirms the conclusion drawn from XANES analysis that the Mn neighbourhood is amorphous here. This shell is mainly populated by the Ga atoms but some traces of the Mn atoms can also be fitted here. As was expected, the

implantation with high energy ions leads to a lack of a long range order around the implanted ions.

After annealing in Ar atmosphere the amplitude of the first shell became higher and the second shell can be distinguished (Fig. 10). The annealing enabled to reconstruct the crystalline structure around the implanted ions; however, still the structure is not the MnSb or GaSb. The Mn atoms are no longer located in the first shell. The Ga atoms dominate in the near neighbourhood forming contracted Ga lattice as it was shown for the samples with low Mn doses. However, in this case there are no traces of the Mn-O bonds and still no Sb atoms were found around Mn.

In the attempt to reintroduce the Sb atoms into the crystal, next two implanted samples were annealed in vacuum with Sb vapour at 400 °C for 48 h and at 600 °C for 2h. The distributions of the elements as measured by SIMS are presented in Fig. 11. Clear attenuation in the depth profiles of the Ga and Sb atoms reflects the disturbed region in the crystal. Therefore, the ratio between the Sb and Ga atoms distributions is taken into consideration in the analysis while investigating the relative changes in the concentration of Sb atoms.

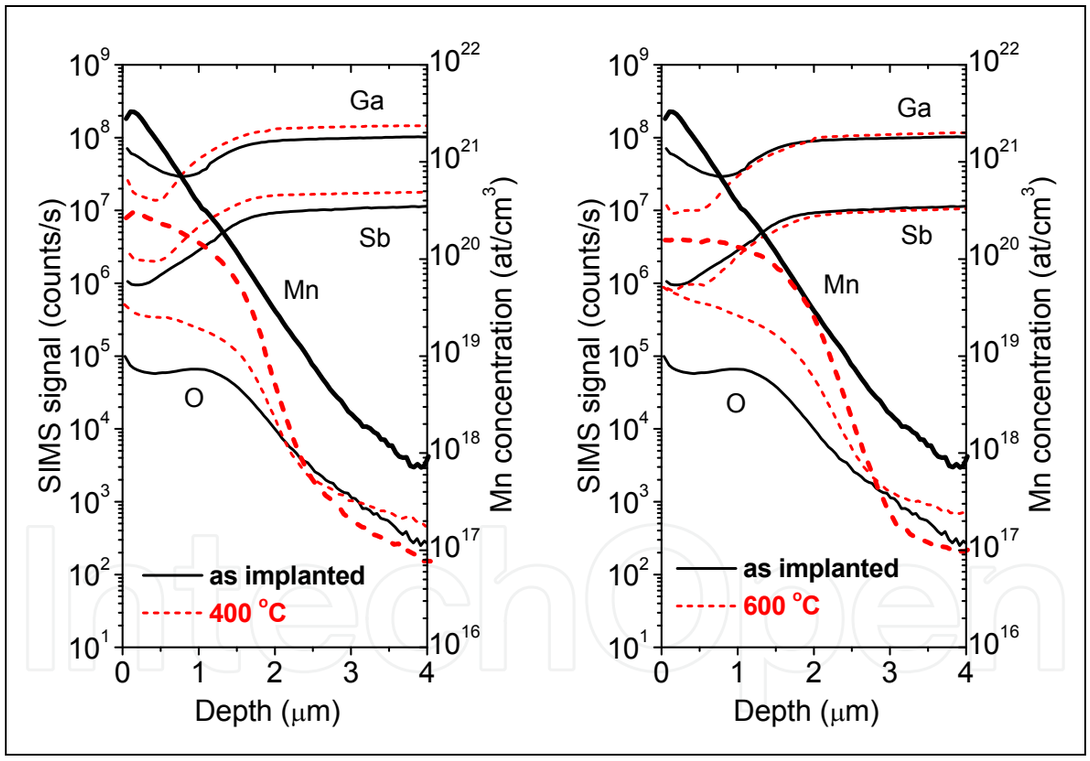

Fig. 11. SIMS depth profiles of the element distribution in the samples annealed in Sb vapour compared with the profiles for the as implanted sample.

SIMS data show that there is a depletion in the distribution of the Sb atoms in respect to the Ga atoms in the vicinity of the surface for the as implanted sample. For the samples annealed in Sb vapour the ratio of the Ga to Sb atoms stays almost constant. It confirms that such annealing reintroduces the Sb atoms into the implanted samples. On the other hand, together with antimony high amount of oxygen was also introduced during this procedure.

EXAFS analysis of the samples annealed in Sb vapour shows completely different atomic order around Mn atoms in comparison to previously investigated samples. It was found from SIMS data that high amount of oxygen was introduced during the heat treatment. And indeed, as seen from the EXAFS spectra in Fig. 12, the first shells show the distribution characteristic for oxides. However, in both samples the Mn atoms don't form stoichiometric MnO with long range order but the oxygen atoms are found in the first shell and different numbers of Mn atoms in the second one. What's more, the Mn-Mn distances differ between the samples annealed at 400 °C (R = 3.12 Å) and 600 °C (R = 3.55 Å) which means that different types of manganese oxides start to be forming.

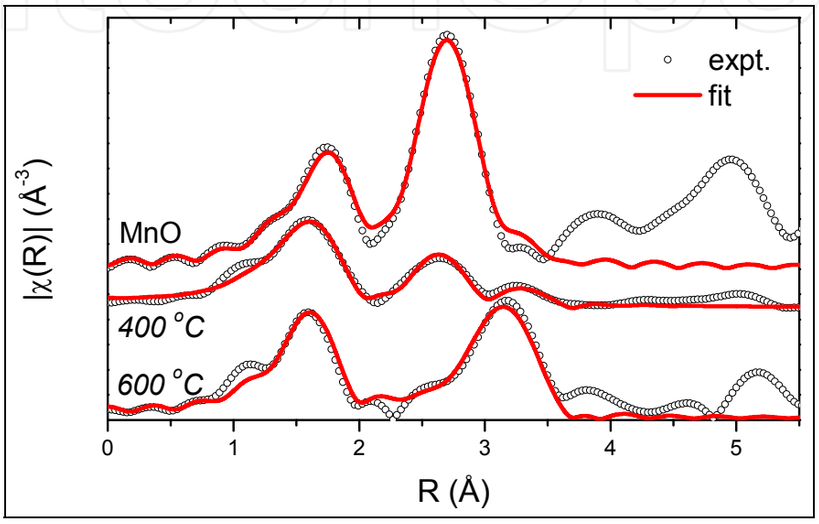

Fig. 12. Fitting results of the FT EXAFS spectra for the samples annealed in Sb vapour compared with the MnO reference. Spectra are shifted vertically for clarity.

In summary, the EXAFS results showed that in all considered cases the implantation removed the Sb atoms from the neighbourhood of the Mn atoms. After annealing in Ar atmosphere the Mn-Ga inclusions were formed. The annealing in Sb vapour reintroduced Sb atoms but together with oxygen which is more reactive and was bounded to the Mn atoms forming Mn oxides (Wolska et al., 2010).

3.3 Implantation with high energy Mn^+ ions (150 keV) at low temperature (80 K) with noble gases co-implantation

The attempts shown above revealed that, in order to establish the proper procedures, it is necessary to investigate processes with more steps. It was assumed that the cold and disordered matrix would prevent the escape of the Sb atoms. Therefore, the co-implantation of noble gases was considered. The He^+ and Ne^+ ions were used to make the matrix disordered. Then, the Mn^+ or the Mn^+ and Sb^+ ions were implanted. The substrates' temperature during the implantation processes was kept at 80 K. The energy and doses of Mn^+ and Sb^+ ions were chosen according to the depth profile ion distribution simulated by the SRIM2008 code (Ziegler et al., 1985) in order to locate the Mn^+ and Sb^+ ions at the distance from 50 to 150 nm below the surface. The implantation of noble gases was assumed not to influence the GaSb matrix density. The calculated ranges of ions are listed in Tab. 2.

Four series of implantation were prepared:

a. *NeMn* where the substrate was implanted first with the Ne^+ ions (250 keV, dose $5x10^{16}$ cm^{-2}) and then with the Mn^+ ions (150 keV, dose $9x10^{14}$ cm^{-2}).
b. *NeMnSb* where after the procedure described in point a) the Sb^+ ions (250 keV, dose $9x10^{14}$ cm^{-2}) were implanted
c. *HeMn* where the substrate was implanted first with the He^+ ions (80 keV, dose $5x10^{13}$ cm^{-2}) and then with the Mn^+ ions (150 keV, dose $9x10^{14}$ cm^{-2}).
d. *HeMnSb* where after the procedure described in point c) the Sb^+ ions (250 keV, dose $9x10^{14}$ cm^{-2}) were implanted.

	I step (noble gases)	II step (Mn^+ ions)	III step (Sb^+ ions)
NeMn	Ne+ GaSb Rp=369.1 nm ΔRp=149.2 nm	Mn+ GaSb Rp=94.82 nm ΔRp=48.11 nm	
NeMnSb	Ne+ GaSb Rp=369.1 nm ΔRp=149.2 nm	Mn+ GaSb Rp=94.82 nm ΔRp=48.11 nm	Sb+ GaSb Rp= 74.20 nm ΔRp= 33.70 nm
HeMn	He+ GaSb Rp= 433.6 nm ΔRp= 151.4 nm	Mn+ GaSb Rp= 94.70 nm ΔRp= 48.28 nm	
HeMnSb	He+ GaSb Rp= 433.6 nm ΔRp= 151.4 nm	Mn+ GaSb Rp= 94.70 nm ΔRp= 48.28 nm	Sb+ GaSb Rp= 78.10 nm ΔRp= 37.30 nm

Table 2. The calculated ranges of ions for each implanted series.

Each of the implanted samples was subsequently divided in two parts. One part was left as such (as-implanted), the second part was subject to rapid thermal annealing (RTA) for 5 min. in Ar atmosphere at the temperature 350 °C (RTA 350).

The SIMS measurements were conducted on the samples annealed at 350 °C. The results are shown in Fig. 13. There are clear differences in the distribution of the elements depending on the type of noble gas used in the co-implantation. What's more, in all cases a considerable amount of oxygen atoms was incorporated deeply into the matrix.

Close comparison of the Mn and Sb distributions found from SIMS measurements with those calculated by the SRIM code confirms that the results depend on the matrix preparation. In Fig. 14 the SRIM and SIMS data for the NeMn and NeMnSb samples are presented. In case of the Mn atoms there is a perfect agreement - the maximum of the concentration is located around 85 nm from the surface for the calculations and 90 nm for the measurements. The maximum for the Sb atoms is supposed to be around 70 nm. From SIMS data it is hard to determine the maximal point but comparison between the NeMn and NeMnSb clearly shows that additional Sb atoms are located within the same depth as the Mn atoms. This could suggest that at least in the NeMnSb sample the possibility of the MnSb formation exists.

In case of the samples co-implanted with the He+ ions the changes introduced to the matrix resulted in remarkable distortion from predicted Mn and Sb distributions. In Fig. 15a it can be seen that according to the calculations the maximum of the concentration should be

around 85 nm for Mn and 70 nm for Sb. However, SIMS results (Fig. 15b) show that for the HeMn sample maximum of the Mn concentration is around 200 nm, while for the HeMnSb sample there is a long plateau slightly tilted down. The results are in correlation neither to the Mn atoms nor to the predictions.

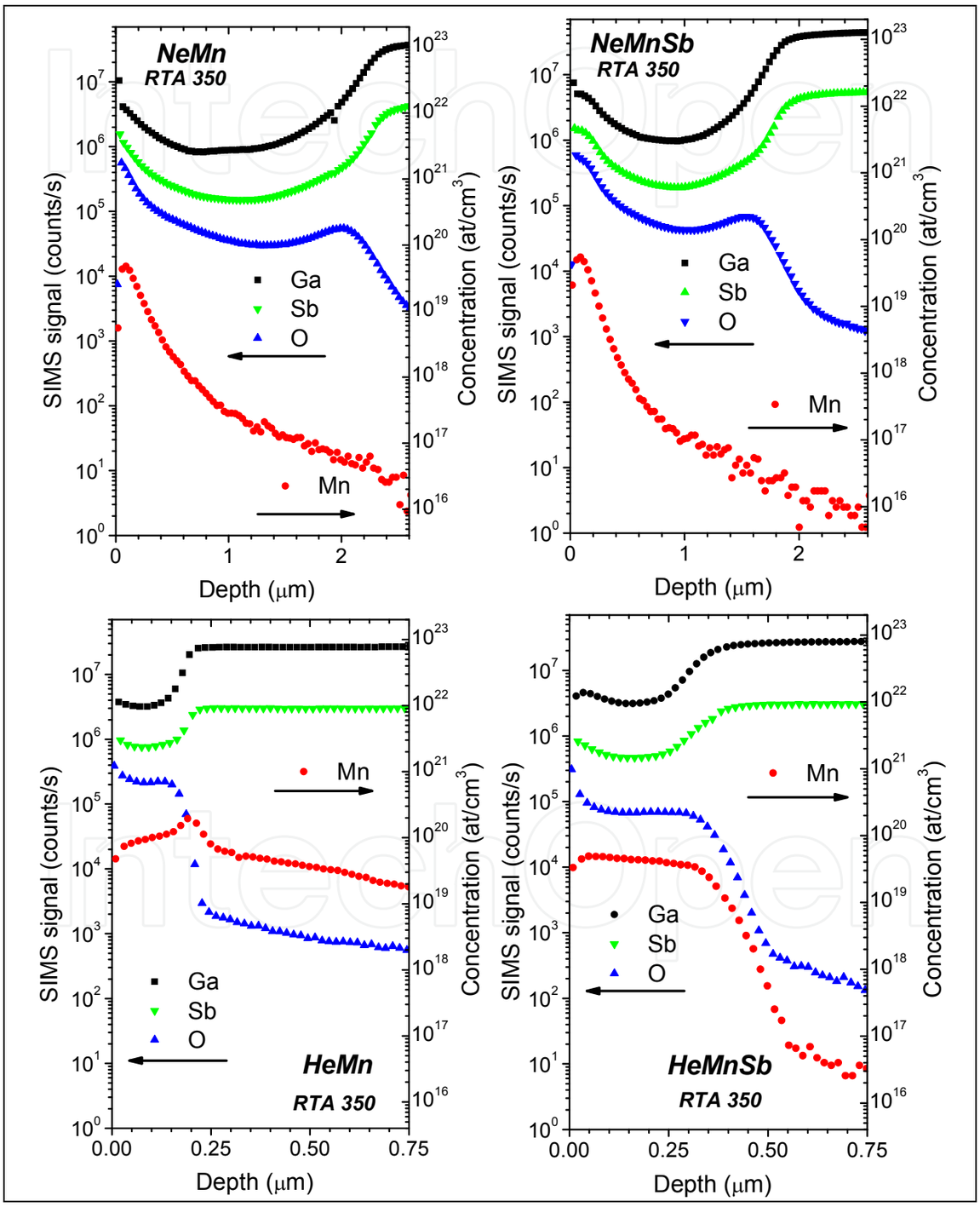

Fig. 13. SIMS depth profiles of the element distribution in the RTA 350 samples.

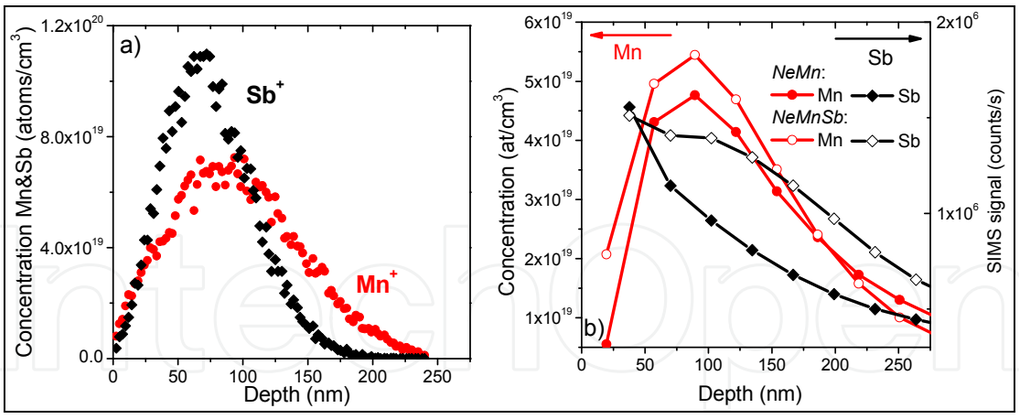

Fig. 14. a) Depth distribution of the implanted Mn and Sb atoms (after the Ne^+ implantation) as calculated by SRIM 2008; b) Depth distribution of Mn and Sb atoms in the samples as measured by SIMS.

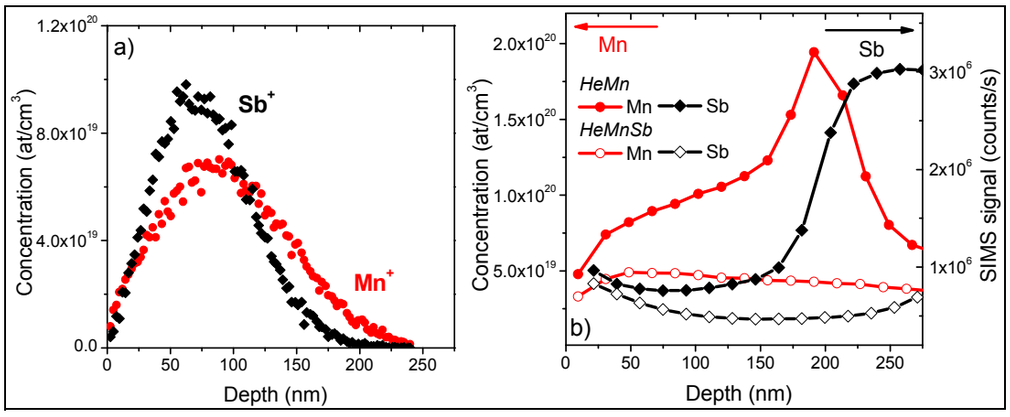

Fig. 15. a) Depth distribution of the implanted Mn and Sb atoms (after the He^+ implantation) as calculated by SRIM 2008; b) Depth distribution of Mn and Sb atoms in the samples as measured by SIMS.

From the analysis conducted above it can be concluded that the distribution of the Mn ions after the implantation by the Ne^+ ions is close to the prediction of SRIM2008 simulation, while changes introduced to the matrix by the He^+ ions resulted in remarkable distortion from predicted Mn distribution. Taking into account that the SIMS results for the NeMnSb sample show that the co-implantation of the Mn^+ and Sb^+ ions tends to gather them in the same region one can suspect that in this sample the MnSb compound may be formed.

The XANES measurements of the as implanted and RTA 350 samples are presented in Fig. 16. The MnSb spectrum is shown for comparison. It is obvious that the MnSb inclusions were not formed, even for the prospective NeMnSb sample. What's more, spectra for all look very similar which indicates that the Mn neighbourhood doesn't change much for any of them.

In Fig. 17 the FT EXAFS spectra for the RTA 350 samples are presented (the spectra of the as implanted samples look very similar and are not shown here). For all of them only the first peak can be distinguished. It means that the neighbourhood of the Mn atoms is amorphous

or highly disordered. The MnO reference spectrum is shown for comparison. Its first shell consisting of oxygen looks like the one in the samples. The second, Mn consisting shell, is not formed in the samples.

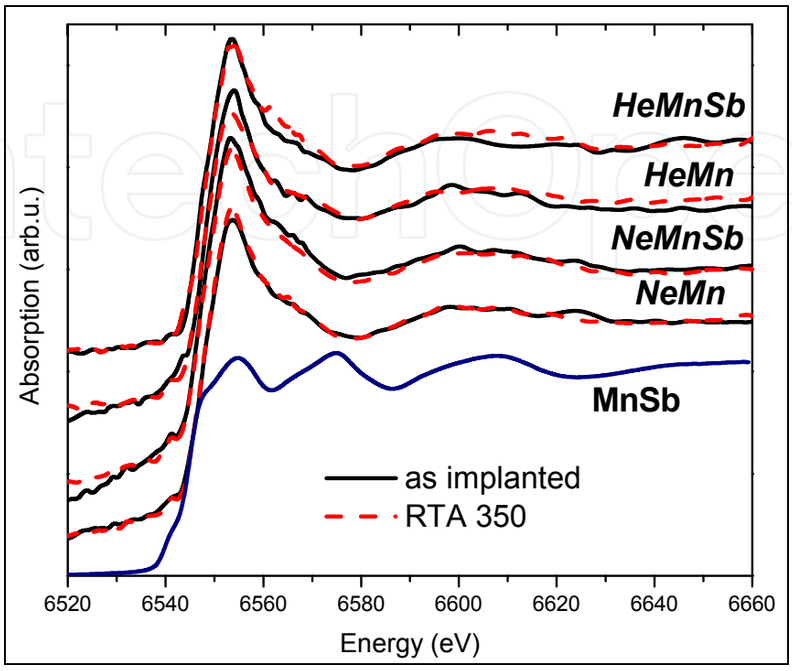

Fig. 16. XANES spectra of the as implanted and annealed samples compared with the MnSb reference. Spectra are shifted vertically for clarity.

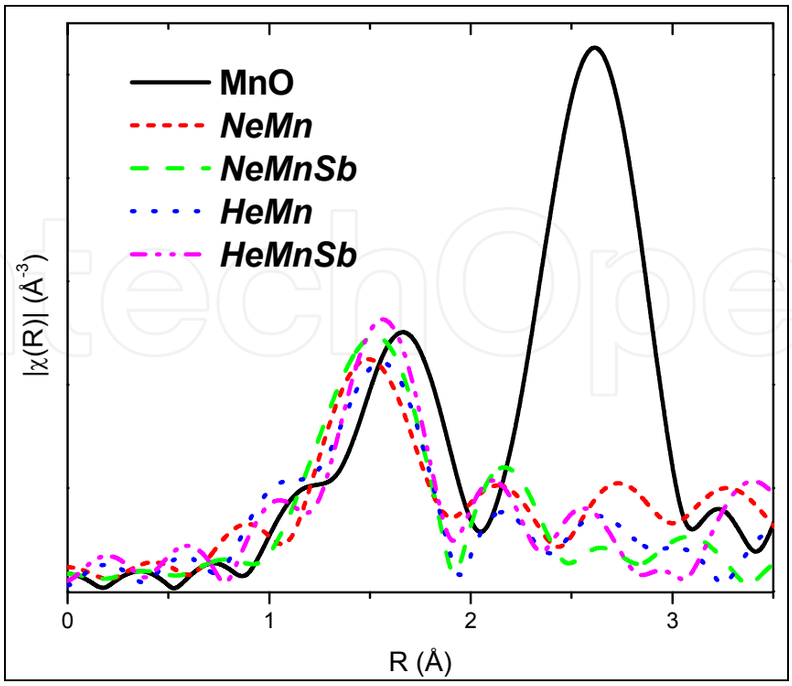

Fig. 17. FT EXAFS spectra for the RTA 350 samples compared with the MnO reference.

The model fitted to the spectra confirms that for all samples Mn-O bonds are formed. In all cases number of the O atoms is lower than for MnO (around 3 atoms instead of 6) and the Mn-O distances are shorter (around 2.03 Å instead of 2.22 Å).

In summary, the X-ray absorption analysis showed that independently on the co-implantation and post-implantation procedures only the Mn oxides were formed inside the GaSb matrix in the considered samples. The implantation into the cold and amorphous substrate indeed prevented the Sb atoms from escaping, however, at the same time through the formed frozen channels the oxygen atoms were incorporated deeply into the matrix.

3.4 Implantation with high energy Mn^+ ions (350 keV) into the Si_3N_4 capped samples

The procedures described above succeeded in preventing the Sb atoms from escaping but did not prevent the oxygen contamination. Therefore, in the next attempt the GaSb (100) crystals were capped with amorphous Sb and Si_3N_4 before the implantation of the Mn ions. The Si_3N_4 cap was supposed to protect the matrix from the introduction of oxygen while the Sb layer was providing additional Sb atoms. The implantation energy was equal to 350 keV and the dose was $1.3x10^{17}$ Mn/cm^2. The substrate temperature during implantation was kept below 50 ^oC. One of the implanted samples was left untreated; the other one was annealed at 500 ^oC for 20 minutes. Additionally, another not capped GaSb(100) crystal was submitted to the same implantation and post-implantation process in order to check the influence of the capping layer. Tab. 3 lists the names of the samples and the processes they were submitted to.

sample	not capped	capped
as implanted	210	210N
annealed	210V	210NV

Table 3. The names of the implanted samples and the processes they were submitted to.

The SIMS measurements show that indeed the presence of the Si_3N_4 capping layer introduces changes between the samples. In case of the capped samples, the depletion in the Ga and Sb distributions ends earlier that in the analogous uncapped ones. (Fig. 18)

For the as-implanted 210 and 210N samples the Mn and O distributions look rather similar. However, in case of the annealed ones the differences are quite significant. For the uncapped 210V sample the Mn and O distributions changed slightly the slope but still remained approximately parallel. For the capped annealed 210NV sample the O atoms were moved closer to the surface while the Mn atoms stayed deeper. It means that capping and annealing indeed had influence on the Mn and O atomic distributions.

Consideration of the SIMS data leads to the conclusion that in the 210NV sample new type of inclusions can be formed. However, in the XANES spectra only slight changes in the shapes are seen between the as implanted and annealed samples independently from the presence of the capping layer (see Fig. 19). The pronounced first peak characteristic for the manganese oxides dominated in the spectra.

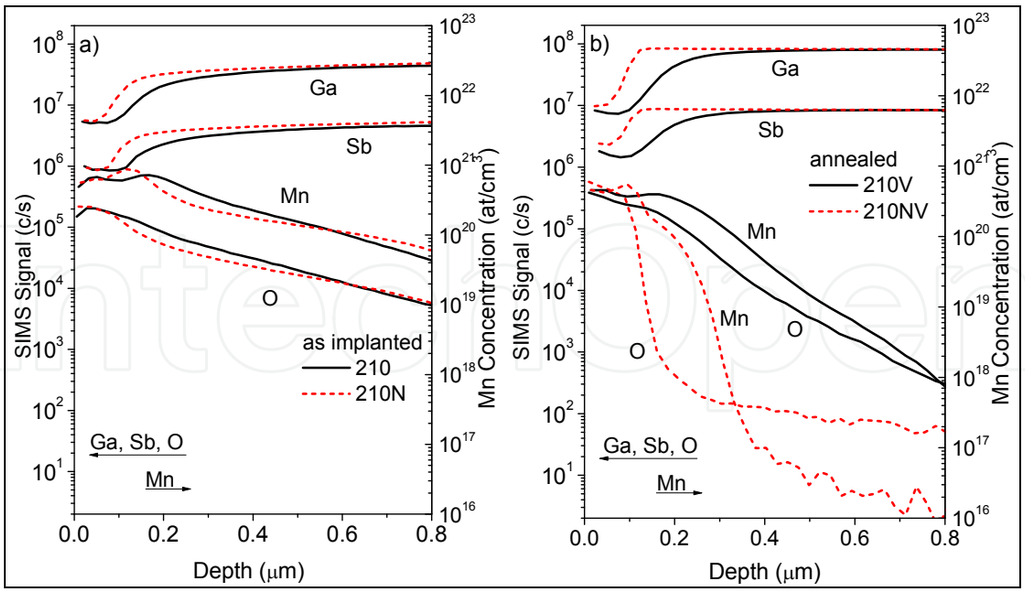

Fig. 18. SIMS depth profiles of the element distribution: a) in the as implanted samples; b) in the samples annealed in Ar atmosphere.

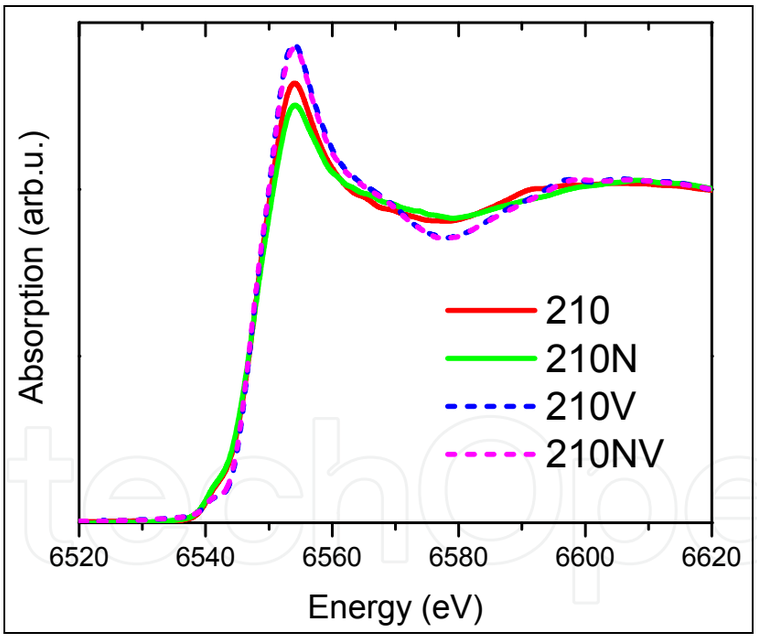

Fig. 19. XANES spectra of the as implanted and annealed samples.

FT EXAFS spectra reveal that in all samples an amorphous neighbourhood exists around the Mn atoms (see Fig. 20). Only first coordination shell is visible. Its amplitude differs between the as-implanted and annealed samples confirming differences noticed in the XANES spectra.

The model fitted to the spectra revealed that the Mn atoms' neighbourhood consists of O atoms. For the as-implanted samples there are in average 3 O atoms at the average distance of 2.09 Å, while for the annealed samples around 5 O atoms can be found at the same distance.

In summary, the SIMS measurements show that the capping layer influenced the distribution of the elements. However, the XAFS analysis reveals that the implantation temperature was too low to enable formation of the inclusions other than the manganese oxides.

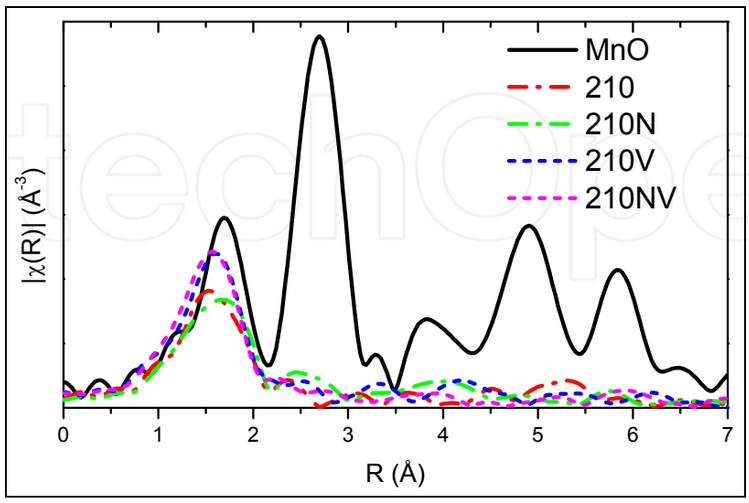

Fig. 20. Magnitude of FT EXAFS spectra for the samples compared with the MnO reference.

3.5 Implantation into warm substrate

Conclusions from the previous procedures suggested another approach - the implantation into the warm substrate. In this case the substrates were kept at 70 °C and 200 °C during the implantation. First, the Mn^+ ions (120 keV, dose $5x10^{16}$ cm^{-2}) were implanted and then the Sb^+ ions (240 keV, dose $5x10^{16}$ cm^{-2}). After implantation the samples were annealed in situ at 350 °C for 0.5 h.

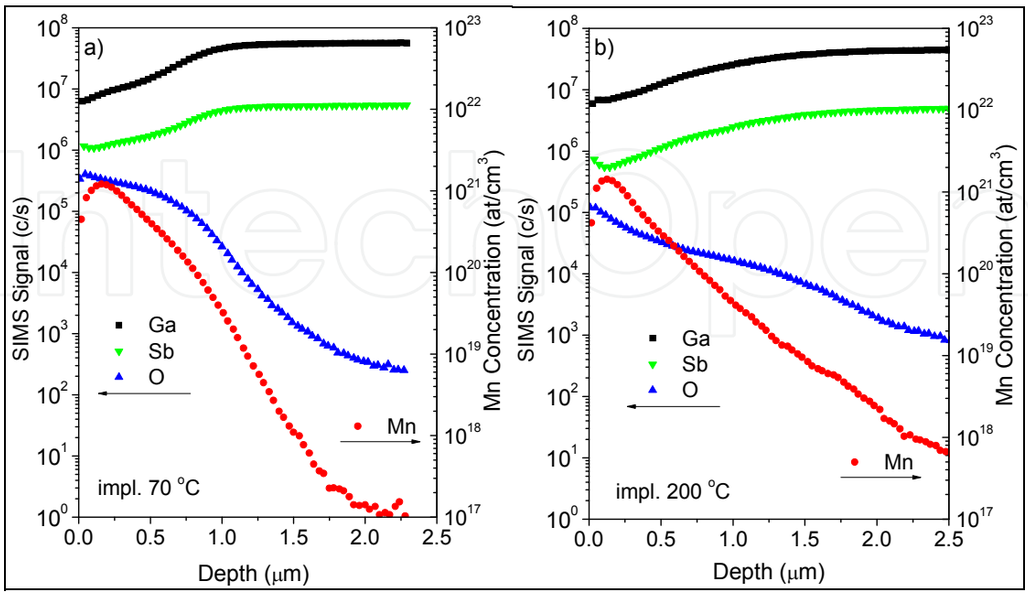

Fig. 21. SIMS depth profiles of the element distribution: a) in the sample implanted at 70 °C; b) in the sample implanted at 200 °C.

From the SIMS data the differences between the samples can be distinguished. For the 200 °C sample the maximum of the Mn atoms concentration is 50 nm closer to the surface than for the 70 °C sample and corresponds with the depletion in the Sb atoms distribution. For the 70 °C sample no depletion in the Sb profile in respect to the Ga one can be detected but the level of the O atoms is higher than in the 200 °C sample.

The XANES spectra confirm that there are differences between the samples (see Fig. 22). Comparison with the previously analysed various types of spectra leads to the conclusions that in the 70 °C sample some oxides can be expected while the 200 °C sample is probably the Mn-Ga type.

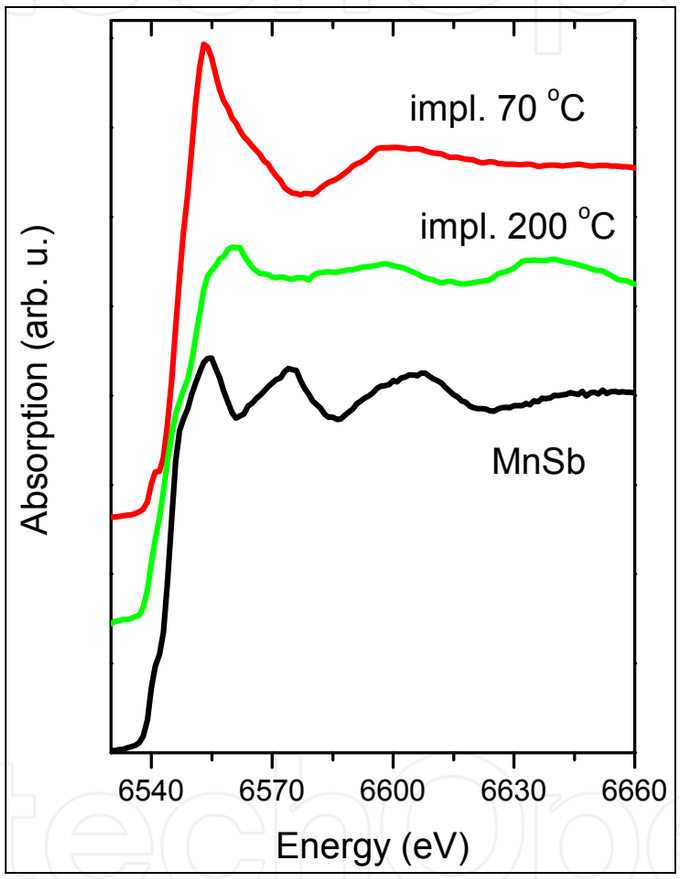

Fig. 22. XANES spectra of the samples implanted at 70 °C and 200 °C compared with the MnSb reference. Spectra are shifted vertically for clarity.

The EXAFS analysis confirms these conclusions. In the 70 °C sample two shells can be distinguished, see Fig. 23. The first one consists of the O atoms at the distance of 2.06 Å. In the second one the Ga atoms are present at the distance of 2.46 Å. In case of the 200 °C sample, according to predictions, two shells containing the Ga atoms are visible (Fig. 24).

It was assumed that the additional Sb atoms introduced into the matrix would facilitate the formation of the MnSb inclusions; however, the EXAFS analysis didn't confirm the presence of the Sb atoms in the Mn atoms' neighbourhood. In case of the sample implanted at 70 °C, the Mn oxides and Mn-Ga clusters coexist. For the sample implanted at 200 °C only the Mn-

Ga clusters are formed. It can be concluded that the thermal disorder during the implantation at higher temperature prevented the migration of the oxygen atoms due to the quick recrystallization of the matrix during cooling. However, the chemical affinity of Mn to Sb is lower than to Ga.

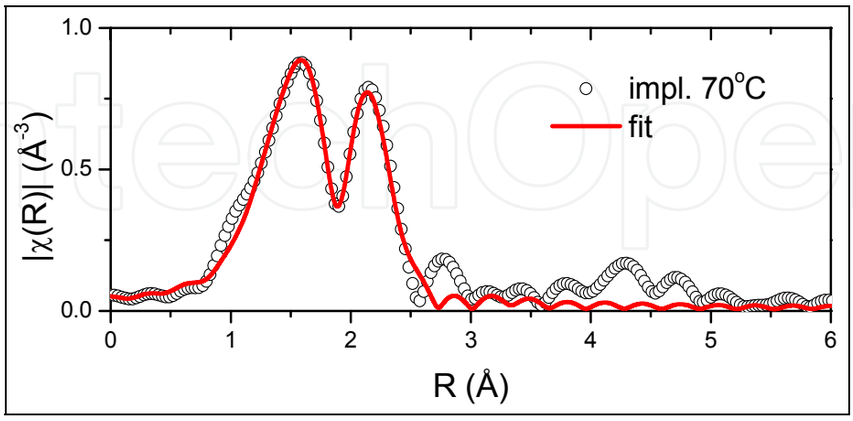

Fig. 23. Magnitude of the FT EXAFS spectrum of the sample implanted at 70 °C together with the fit. In the first shell the oxygen, in the second - the gallium atoms are located.

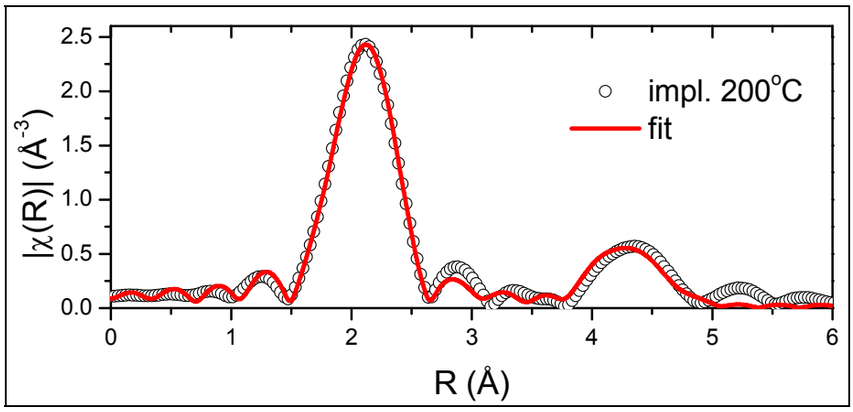

Fig. 24. Magnitude of the FT EXAFS spectrum of the sample implanted at 200 °C together with the fit. The first and second shells consist of the gallium atoms.

4. Conclusions

The examples of forming the MnSb inclusions in the GaSb crystals during the Mn^+ ion implantation shown in this chapter demonstrate that detailed information about the dopants' neighbourhood is a very important part of characterization of any new material. The attempts at obtaining the MnSb inclusions encountered several obstacles which were recognized by XAFS analysis. Implantation tends to remove Sb atoms from the neighbourhood of the Mn atoms even with the implantation temperature kept close to liquid nitrogen temperature. It was possible to reintroduce Sb atoms by the annealing in Sb vapour but together with oxygen which is more reactive and was bounded to the Mn atoms. Keeping the high temperature during the implantation prevented the migration of oxygen but still the chemical affinity of Mn to Sb is lower than to Ga and the Mn-Ga clusters are formed.

In summary, the theoretical calculations enable to determine the values of the implantation parameters in order to plan distribution of each element. Thanks to the SIMS measurements it can be checked if the element distributions are in agreement with the predictions. However, it is not enough to ensure that the implanted element is located in the right part of the material, it is also important to find out its chemical bonding which is possible with the XAFS techniques.

5. Acknowledgments

The author would like to acknowledge Dr. R. Jakiela from Polish Academy of Sciences in Warsaw for the SIMS measurements and Dr. M. Kulik from University Maria Curie-Skłodowska in Lublin for performing the SRIM calculations and some of the implantation procedures. The author would also like to thanks Dr. A. Hallen from Royal Inst. of Technology in Sweden and Dr. D. Arvanitis from Uppsala University in Sweden for advice and help in starting the GaSb implantation project.

This work was partially supported by national grant of Ministry of Science and High Education N202-052-32/1189. The synchrotron research leading to these results has received funding from the European Community's Seventh Framework Programme (FP7/2007-2013) under grant agreement n° 226716.

6. References

Croft, M.; Sills, D.; Greenblatt, M.; Lee, C.; Cheng, S.-W.; Ramanujachary, K.V. & Tran, D. (1997). Systematic Mn d-configuration change in the $La_{1-x}Ca_xMnO_3$ system: A Mn K-edge XAS study. *Phys. Rev. B,* Vol. 55, No. 14, pp. 8726–8732.

Eisenberger, P. & Kincaid, B.M. (1978). EXAFS: new horizons in structure determinations. *Science*, Vol. 200, No. 4349, pp. 1441-1447.

Hai, P.N.; Ohya, S.; Tanaka, M.; Barnes, S. E. & Maekawa, S. (2009). Electromotive force and huge magnetoresistance in magnetic tunnel junctions. *Nature,* Vol. 458, No. 7237, pp. 489-492.

Koningsberger, D.C. & Prins, R. (Ed.) (1988). X-ray Absorption. John Wiley and Sons Inc., New York.

Lawniczak-Jablonska, K.; Wolska, A.; Klepka, M.T.; Kret, S.; Gosk, J.; Twardowski, A.; Wasik, D.; Kwiatkowski, A.; Kurowska, B.; Kowalski, B. J. & Sadowski J. (2011). Magnetic Properties of MnSb Nano-inclusions Formed in GaSb Matrix Directly During MBE Process. *J. Appl. Phys.,* Vol. 109, No. 7, pp. 074308-1 - 074308-7.

Lee, P.A.; Citrin, P.H.; Eisenberger, P. & Kincaid, B.M. (1981). Extended x-ray absorption fine structure—its strengths and limitations as a structural tool. *Rev. Mod. Phys.,* Vol. 53, No. 4, pp. 769–806.

Panchula, A.F.; Kaiser, C.; Kellock, A. & Parkin, S.S. (2003). Spin polarization and magnetotransport of Mn–Sb alloys in magnetic tunnel junctions. *Appl. Phys. Lett.*, Vol. 83, No. 9, pp. 1812-1814.

Ravel, B. & Newville, M. (2005). ATHENA, ARTEMIS, HEPHAESTUS: data analysis for X-ray absorption spectroscopy using IFEFFIT. *J. Synchrotron Rad.,* Vol. 12, No. 4, pp. 537-541.

Stohr, J. (1996). NEXAFS spectroscopy. Springer-Verlag. ISBN 3-540-54422-4 Berlin, Heidelberg, New York.

Teo, B.K. (1986). EXAFS: Basic Principles and Data Analysis. Springer-Verlag, ISBN 0-387-15833-2 Berlin, Heidelberg, New York, Tokyo.

Teo, B.K. & Joy, D.C. (Ed.) (1981). EXAFS Spectroscopy. Plenum Press. ISBN 0-306-40564-3 New York and London.

Wolska, A.; Lawniczak-Jablonska, K.; Klepka, M.T.; Barcz, A.; Hallen, A. & Arvanitis, D. (2010). Study of the local environment of Mn ions implanted in GaSb. *Acta Phys. Pol. A,* Vol. 117, No. 2, pp. 286-292.

Wolska, A.; Klepka, M.T.; Lawniczak-Jablonska, K.; Sadowski, J.; Reszka, A. & Kowalski B.J. (2011). MnSb inclusions in the GaSb matrix studied by X-ray absorption spectroscopy. *Radiat. Phys. Chem.,* Vol. 80, No. 10, pp. 1026-1030.

Ziegler, J.F.; Biersack, J.P. & Litmar U. (1985). SRIM—The Stopping and Range of Ions in Solids. Pergamon Press, New York.

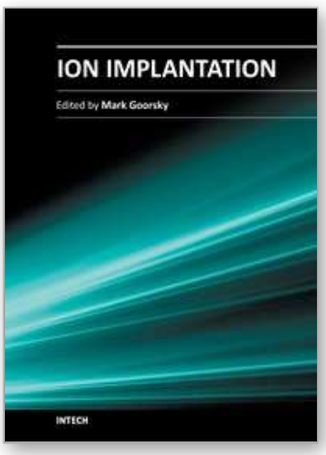

Ion Implantation

Edited by Prof. Mark Goorsky

ISBN 978-953-51-0634-0
Hard cover, 436 pages
Publisher InTech
Published online 30, May, 2012
Published in print edition May, 2012

Ion implantation presents a continuously evolving technology. While the benefits of ion implantation are well recognized for many commercial endeavors, there have been recent developments in this field. Improvements in equipment, understanding of beam-solid interactions, applications to new materials, improved characterization techniques, and more recent developments to use implantation for nanostructure formation point to new directions for ion implantation and are presented in this book.

How to reference

In order to correctly reference this scholarly work, feel free to copy and paste the following:

Anna Wolska (2012). Determination of Near-Neighbour Bonding in the Mn-Implanted GaSb Crystals, Ion Implantation, Prof. Mark Goorsky (Ed.), ISBN: 978-953-51-0634-0, InTech, Available from: http://www.intechopen.com/books/ion-implantation/determination-of-near-neighbour-bonding-in-the-mn-implanted-gasb-crystals

INTECH
open science | open minds

InTech Europe
University Campus STeP Ri
Slavka Krautzeka 83/A
51000 Rijeka, Croatia
Phone: +385 (51) 770 447
Fax: +385 (51) 686 166
www.intechopen.com

InTech China
Unit 405, Office Block, Hotel Equatorial Shanghai
No.65, Yan An Road (West), Shanghai, 200040, China
中国上海市延安西路65号上海国际贵都大饭店办公楼405单元
Phone: +86-21-62489820
Fax: +86-21-62489821

IntechOpen